# A Segmented Traction Drive System with a Small dc Bus Capacitor

Gui-Jia Su and Lixin Tang
Energy and Transportation Science Division
Oak Ridge National Laboratory
Knoxville, TN, USA
sugj@ornl.gov

***Abstract*— The standard voltage source inverter (VSI), widely used in electric vehicle/hybrid electric vehicle (EV/HEV) traction drives, requires a bulky dc bus capacitor, typically made of polypropylene films, to absorb the large ripple currents generated by the pulse width modulated switching actions and prevent them from damaging and shortening the battery's life. The dc bus capacitor presents a significant barrier to meeting the U.S. DRIVE targets for cost, volume, and weight for inverters. Currently the dc bus capacitor contributes up to 20% of the cost and weight of an inverter and up to 30% of an inverter's volume. The large ripple currents become even more problematic for the film capacitors (the capacitor technology of choice for EVs/HEVs) in high temperature environments as their ripple current handling capability decreases rapidly with rising temperatures. There is thus an urgent need to reduce the ripple currents. This paper presents a segmented traction drive system that can significantly decrease the ripple currents and thus the size of the dc bus capacitor.**

## I. INTRODUCTION

The dc bus capacitor is an indispensable component for maintaining a stable dc bus voltage and smooth battery current for voltage source inverter (VSI) based traction drive systems in electric vehicles (EVs), hybrid EVs (HEVs), and plug-in HEVs. The VSI, mainly comprising six power semiconductor switches—typically insulated gate bipolar transistors (IGBTs)—and a dc bus filter capacitor, switches the battery dc voltage to produce a desired set of three phase ac voltages according to a chosen pulse width modulation (PWM) scheme. The ac voltages in turn regulate the motor current to control the motor torque and speed. In doing the switching operations, the inverter generates large ripple components in the dc link current, thus necessitating the use of the dc bus filter capacitor to absorb the ripple currents and suppress voltage transients, which occur on the dc bus at every instant of inverter switching and, if not sufficiently constrained, are detrimental to the battery life and reliability of the semiconductor switches in the inverter. Fig. 1 shows simulated motor currents, $i_a$, $i_b$, and $i_c$; capacitor ripple current, $i_{Cbus}$, and its root-mean-square (rms) value, $i_{Cbus(rms)}$; inverter dc link current, $i_{inv}$; and battery current, $i_{bat}$, in a typical 55 kW HEV inverter. The capacitor ripple current reaches as large as 200 Arms, almost 70% of the motor current. As a result, a bulky and costly dc bus capacitor of about 1,000 μF is required to prevent this large ripple current from flowing into the battery and to maintain a smooth dc bus voltage. Even with the large bus capacitor, there is still a relatively large ripple component of 70 A peak-to-peak in the battery current, $i_{bat}$.

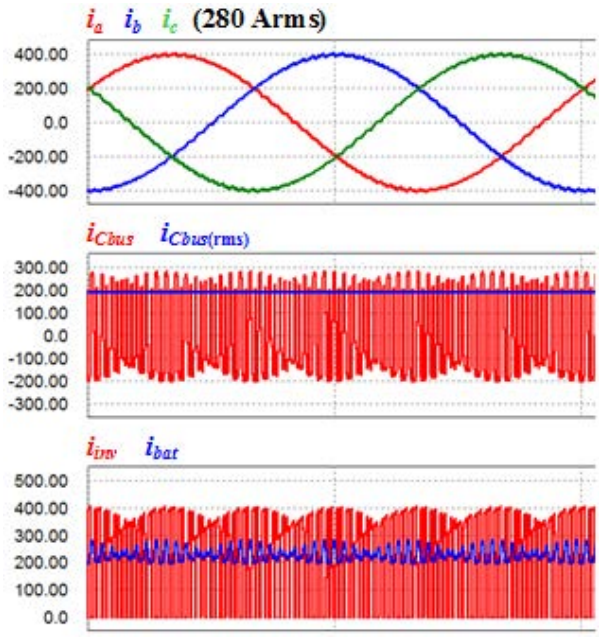


Figure 1. Simulated waveforms in the standard VSI based drive system.

Concerns about the reliability of electrolytic capacitors have forced HEV makers to use self-healing film capacitors, and currently available film capacitors that can meet the demanding requirements are costly and bulky, taking up one-third of the inverter volume and making up one-fifth of the cost.

This manuscript has been authored by UT-Battelle, LLC, under contract DE-AC05-00OR22725 with the U.S. Department of Energy. The U.S. government retains and the publisher, by accepting the article for publication, acknowledges that the U.S. government retains a nonexclusive, paid-up, irrevocable, worldwide license to publish or reproduce the published form of this manuscript, or allow others to do so, for U.S. government purposes.

978-1-4673-0803-8/12/$31.00 ©2012 IEEE

The dc bus capacitor, therefore, presents a significant barrier to meeting the U.S. DRIVE program goals for inverter volume, lifetime, and cost established by the U.S. Department of Energy and its industrial partners [1]. The large ripple currents become even more problematic for the film capacitors in high temperature environments as their ripple current handling capability decreases rapidly with rising temperatures, as indicated in Fig. 2 for one of the best 150 µF film capacitors available on the market [2]. For example, as the ambient temperature rises from 85°C to 105°C, weight, volume, and cost of capacitors could increase by a factor of 5 due to the decrease of ripple current capability from 50 A to 11 A.

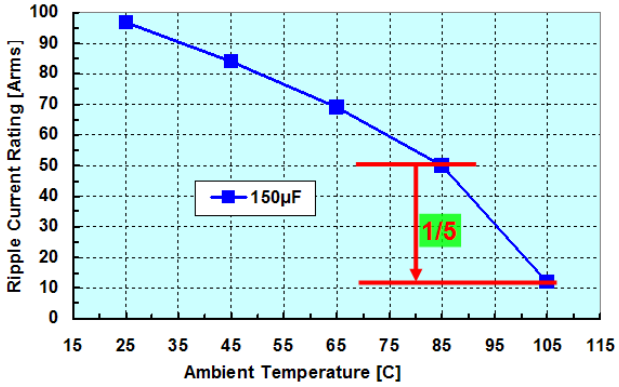


Figure 2. Ripple current capability vs ambient temperature for a high-performance film capacitor [2].

Minimizing the size of this bulky component by significantly reducing the inverter ripple current would thus help achieve the U.S. DRIVE targets. A much smaller dc bus capacitor would also enable inverters to operate at higher temperatures. The following factors, however, make this a difficult task: (1) increasing the switching frequency, which is one of the anticipated benefits with future wide-bandgap-based switches, has little impact on the bus capacitor ripple currents because the capacitor ripple currents depend on the motor peak current, although so increasing switching frequency does reduce the dc bus voltage and motor current ripples, and (2) the major components of the capacitor ripple currents have frequencies of multiples of the switching frequency or their side bands. The high frequency nature of the ripple currents makes it impractical to actively filter out the ripple components because doing so requires the use of very high switching frequencies in the active filter.

This paper presents a segmented traction drive system that does not increase the total silicon area or add passive components but can significantly reduce the ripple current and thus the requirement on bus capacitance. It is based on the segmentation of the inverter switches and the motor windings to form multiple parallel connected drive units and the use of interleaved PWM switching to reduce the dc link ripple current. While the idea of paralleling multiple inverters with coupled or noncoupled output inductors has been reported, it was mainly as a way to scale up inverter system power ratings and reduce the harmonic components in the output currents and the ac output filters [3]–[11] whereas our work is focused on the reduction of the dc bus ripple current. Comprehensive test results are included in this paper to show the effectiveness of the segmented traction drive system in reducing the dc bus ripple current.

## II. Description of the Segmented Traction Drive System

### A. Segmented Traction Drive System

Fig. 3 illustrates a segmented traction drive system that includes a battery, a dc bus filter capacitor, a three-phase inverter, and a three-phase electrical motor/generator. The inverter switches in the power module ($S_1$–$S_6$) and stator windings in the motor are separated into two sets of switches (indicated in red and blue in the figure) and windings ($a_1$, $b_1$, $c_1$) and ($a_2$, $b_2$, $c_2$). Further, each phase group of the stator windings ($a_1$, $a_2$), ($b_1$, $b_2$), and ($c_1$, $c_2$) can be colocated in the same stator slots or displaced in different regions for a multipole motor. Each group of switches (red or blue) is connected as an inverter bridge and connects to one set of the motor stator windings, forming an independent drive unit, as shown in Fig. 4. Because switches in most high power inverter modules are comprised of multiple IGBT and diode dies connected in parallel, only minor modifications to the switch configuration as well as three additional terminals with half the current rating of the original ones are needed to form the segmented arrangement.

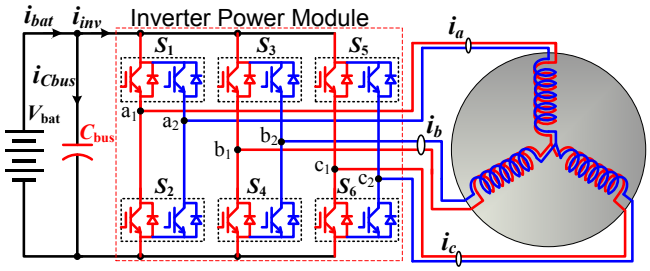


Figure 3. A segmented traction drive system.

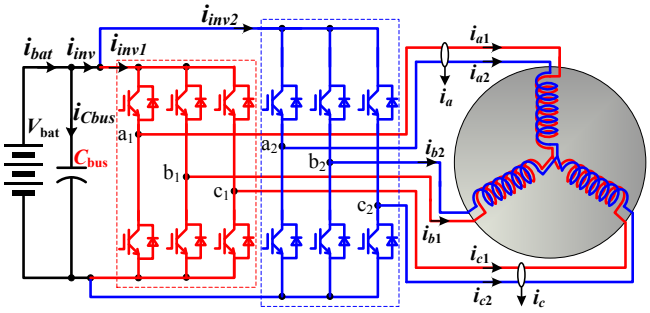


Figure 4. An equivalent arrangment of the segmented traction drive system.

The timing of the turn-on and turn-off of the corresponding switches in the two independent drive units is controlled in a way that minimizes the dc bus ripple currents. Various interleaved carrier based and space vector PWM methods were studied in simulation and tested with both a

resistive load bank and an induction motor to quantify their impacts on the dc bus ripple current. Test results are given in section III.

No changes are needed in the implementation of control of the motor except the modifications in the PWM control of the switches in the inverter. Fig. 5 shows a control block diagram for control of the segmented drive with interleaved PWM switching to minimize the capacitor ripple current and a carrier based interleaved PWM switching scheme. To control the motor speed or torque, two of the combined three phase motor currents, $i_a$ (= $i_{a1}$+ $i_{a2}$), $i_b$ (= $i_{b1}$+ $i_{b2}$), and $i_c$ (= $i_{c1}$+ $i_{c2}$), along with the motor speed or rotor position are sensed and fed to a chosen motor control scheme, which is typically based on the field orientation control. Therefore, no additional current sensors are required, compared to the non-segmented drive. The motor controller produces a set of three phase voltage modulation signals, $v_a$, $v_b$, and $v_c$, which are then compared with two identical carriers with a phase angle displacement, $v_{inv1}$ and $v_{inv2}$, to generate interleaved PWM switching control signals for the two inverter units, $v_{ga1}$, $v_{gb1}$, $v_{gc1}$, and $v_{ga2}$, $v_{gb2}$, $v_{gc2}$. Alternatively, space vector based PWM methods can be used to generate interleaved PWM switching control signals.

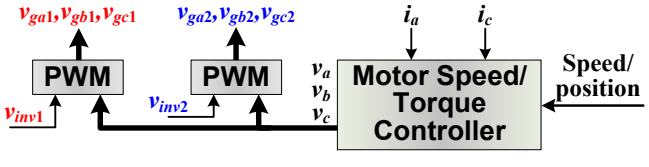


(a) Control block diagram

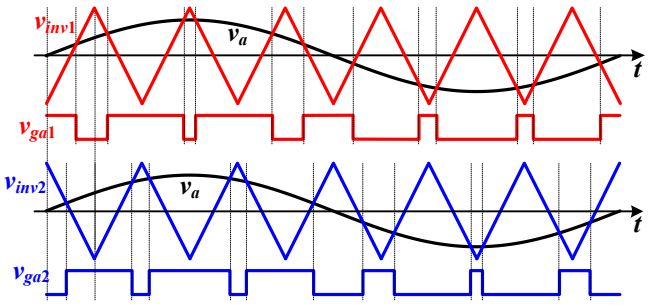


(b) Interleaved PWM switching control based on two identical carriers with a phase angle displacement between them

Figure 5. Control of the segmented drive with interleaved PWM switching to minimize the capacitor ripple current.

### *B. Dc Bus Capacitor Ripple Current Reduction*

The inverter dc link current, $i_{inv}$, in the non-segmented six-switch three phase inverter operating at a switching frequency, $f_{sw}$, and a fundamental frequency, $f_m$, consists of a dc component, $I_{dc}$, and many harmonic components, and can be expressed by

$$i_{inv} = I_{dc} + \sum_{k=0}^{\infty}\sum_{n=1}^{\infty} I_{n,k} \sin[2\pi(nf_{sw} \pm kf_m)t + \alpha_{n,k}], \quad (1)$$

where $I_{n,k}$ and $\alpha_{n,k}$ represent respectively the amplitude and phase angle of the harmonic component identified by the integers, $n$ and $k$. The harmonics should be absorbed by the dc bus capacitor and the sum of them is thus the capacitor ripple current, $i_{Cbus}$. The major components of the capacitor ripple current have frequencies of multiples of the switching frequency ($nf_{sw}$) or their side bands ($nf_{sw}\pm f_m$, $nf_{sw}\pm 2f_m$, …), as in (1). The rms value of the capacitor ripple current, $I_{Cbus(rms)}$, can be calculated by [12]

$$I_{Cbus(rms)} = \sqrt{\frac{M}{4\pi}[2\sqrt{3} + (8\sqrt{3} - 4.5\pi M)\cos^2\varphi]} \cdot I_{m1(rms)}, \quad (2)$$

where $M$ is the modulation index; $\varphi$ the fundamental power factor; and $I_{m1(rms)}$ the rms values of the fundamental motor phase current. The capacitor ripple current can reach over 60 % of the motor current and thus a large bus capacitor of about 1,000 μF is needed for a 55 kW traction drive inverter.

The two inverter dc link currents, $i_{inv1}$, and $i_{inv2}$, and the combined, $i_{inv}$, in the segmented inverter in Fig. 4 can be expressed by

$$i_{inv1} = 0.5\left\{I_{dc} + \sum_{k=0}^{\infty}\sum_{n=1}^{\infty} I_{n,k} \sin[2\pi(nf_{sw} \pm kf_m)t + \alpha_{n,k}]\right\}, \quad (3)$$

$$i_{inv2} = 0.5\left\{I_{dc} + \sum_{k=0}^{\infty}\sum_{n=1}^{\infty} I_{n,k} \sin[2\pi(nf_{sw} \pm kf_m)t + \beta_{n,k}]\right\}, \quad (4)$$

$$i_{inv} = I_{dc} + \sum_{k=0}^{\infty}\sum_{n=1}^{\infty}\sqrt{\frac{1+\cos(\beta_{n,k}-\alpha_{n,k})}{2}} I_{n,k} \times \sin[2\pi(nf_{sw} \pm kf_m)t + \frac{\alpha_{n,k}+\beta_{n,k}}{2}], \quad (5)$$

where $\alpha_{n,k}$ and $\beta_{n,k}$ represent the phase angles of the harmonic components of the two inverters identified by the integers, $n$ and $k$. As shown in the equations above, the amplitude of each combined ripple component can be reduced by introducing a phase shift into the corresponding ripple components of the two drive units to make $\alpha_{n,k}\neq\beta_{n,k}$. Moreover, the combined ripple current components can be reduced to zero by introducing a 180 electrical degree phase shift into the corresponding ripple components of the two drive units. Shifting the relative phase angle of the carrier signals as shown in Fig. 5 can lead to cancellation of some of the ripple current components while reducing others. The net effect is a significantly reduced dc bus ripple current to be filtered out by the dc bus capacitor. As a result of the reduced dc ripple current, the size of the dc bus capacitors can be reduced by 55%-75%. Thus, less costly and less bulky capacitors can be used.

Various interleaved carrier based and space vector PWM methods were studied in simulation and tested with both a resistive load bank and an induction motor to quantify their

impacts on the dc bus ripple current. In the carrier based interleaved PWM switching control illustrated in Fig. 5, the two carrier signals are identical except there is a phase shift between the two signals. It is found that the use of two sawtooth wave shaped carriers with a phase shift of 180 electrical degrees results in the lowest capacitor ripple currents and that of two triangle carriers with a phase shift of 90 electrical degrees produces slightly higher capacitor ripple currents.

### C. *Simulation results*

A simulation study using PSIM was carried out for a PM motor drive in both the segmented and non-segmented arrangements to assess the effect of various PWM schemes on the reduction of ripple current to determine the optimal PWM method. Results for the following five cases are included in this paper: (a) Non-segmented, sawtooth carrier; (b) Non-segmented, triangle carrier; (c) Segmented, triangle carriers of 180 electrical degrees phase shift; (d) Segmented, triangle carriers of 90 electrical degrees phase shift; and (e) Segmented, sawtooth carriers of 180 electrical degrees phase shift.

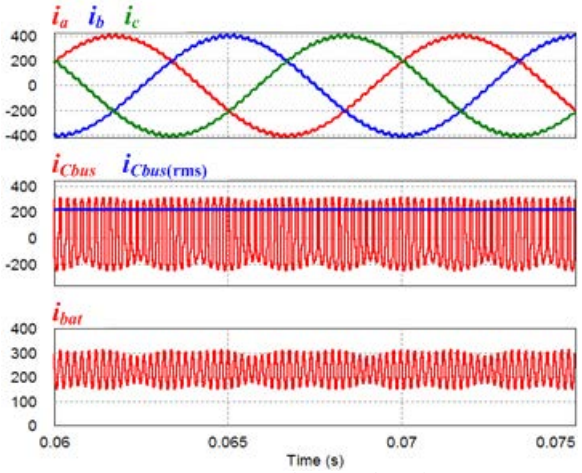


(a) Non-segmented, sawtooth carrier

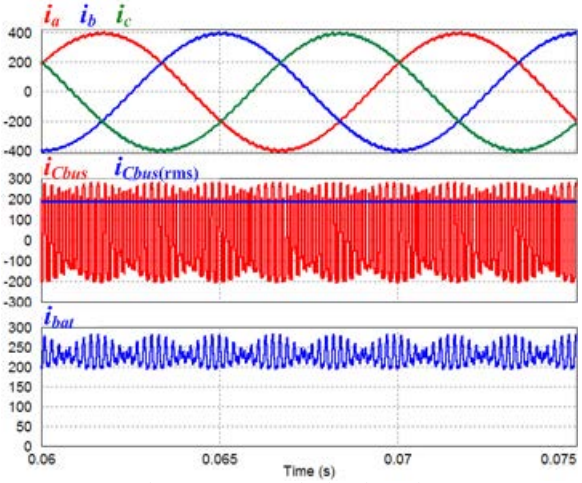


(b) Non-segmented, triangle carrier

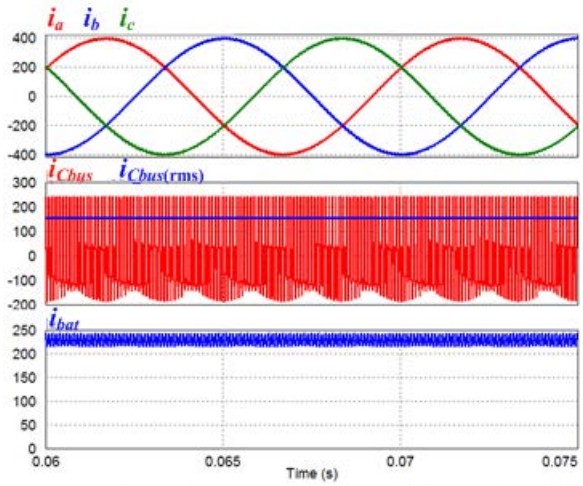


(c) Segmented, triangle carriers of 180 electrical degrees phase shift

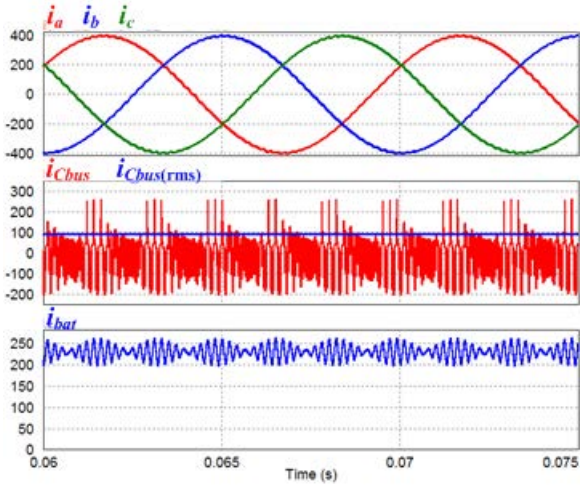


(d) Segmented, triangle carriers of 90 electrical degrees phase shift

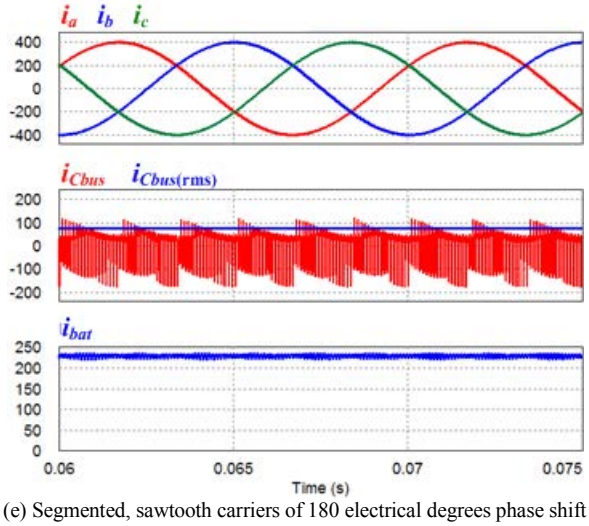


(e) Segmented, sawtooth carriers of 180 electrical degrees phase shift

Figure 6. Simulation results.

Figure 6 shows simulated motor currents, $i_a$, $i_b$, $i_c$, capacitor ripple current, $i_{Cbus}$ and $i_{Cbus(rms)}$, and battery current, $i_{bat}$ at the maximum motor current of 280Arms for the five cases. The calculated capacitor ripple currents are:

(a) 222Arms, (b) 190Arms, (c) 157Arms, (d) 95Arms, and (e) 75Arms. Compared with the case (a), the segmented drive with the optimal PWM scheme (case e) results a 66% reduction in the capacitor ripple current and a significant reduction of battery ripple current: from greater than 100Ap-p to less than 15A.

Figure 7 plots the capacitor ripple currents at various levels of motor current and a fixed motor speed for the five cases. As expected, the capacitor ripple current is proportional to the motor current and the segmented drive with the optimal PWM scheme always generates the lowest capacitor ripple current; less than 35% of that in case (a).

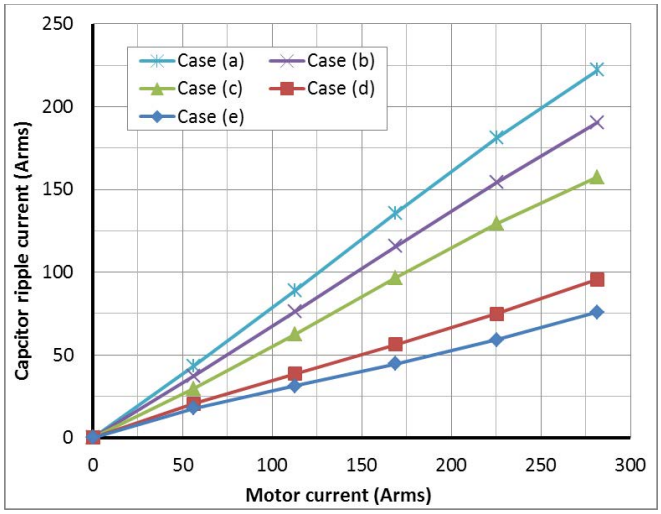


Figure 7. Comparison of capacitor ripple current vs motor current for the following five cases: (a) Non-segmented, sawtooth carrier; (b) Non-segmented, triangle carrier; (c) Segmented, triangle carriers of 180 electrical degrees phase shift; (d) Segmented, triangle carriers of 90 electrical degrees phase shift; and (e) Segmented, sawtooth carriers of 180 electrical degrees phase shift (simulation results).

## III. Test Setup and Experimental Results

### A. Hardware Setup

Incorporating the simulation study, a 55 kW segmented inverter prototype was designed [Fig. 8(a)], built, and tested. A 55 kW baseline non-segmented inverter [Fig. 8(b)] was also designed for comparison. Both designs use the same IGBT modules and the same water-cooled cold plate, measuring 6 in. by 7 in., for fixing and cooling the IGBT modules. Capacitor requirements for the segmented inverter are 400 µF and are fulfilled with two film capacitors, each rated at 500 V and 200 µF. In comparison, a total amount of capacitance of 1,000 µF is needed for the baseline design and is furnished with five of the film capacitors. The capacitors are mounted on an aluminum heat sink attached to the cold plate. Because of the larger capacitance requirement (more than twice that of the segmented inverter), the baseline design requires a significantly larger fixture for mounting the capacitors. Table 1 gives a comparison of heat sink size and capacitor volume for the two designs. Fig. 9 is a photo of the assembled 55 kW segmented inverter prototype. A Texas Instruments 32-bit fixed-point digital signal processor chip, TMS320F2812, was used to implement the motor control and PWM switching schemes.

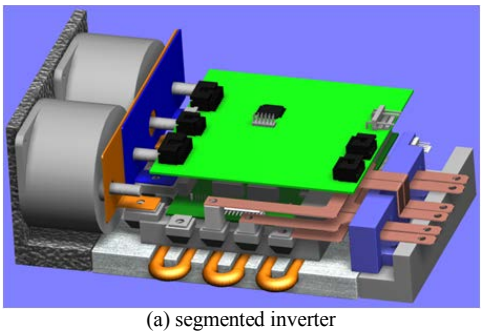

(a) segmented inverter

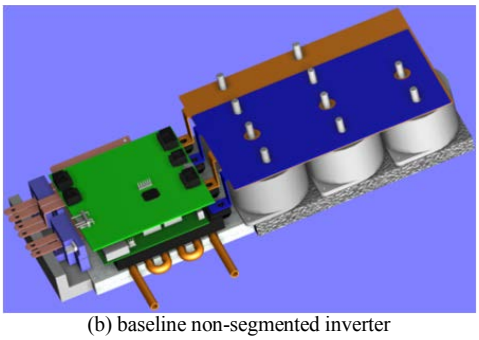

(b) baseline non-segmented inverter

Figure 8. Hardware designs for 55 kW prototypes.

TABLE I. Comparison of Heat Sink Sizes and Capacitor Volumes of 55 kW Segmented Inverter and Baseline Non-Segmented Inverter Designs

| | Baseline | Segmented |
|---|---|---|
| Heat sink footprint | 6”x7”+ 6.6”x9.6” | 6”x7”+ 6.6”x2.2” |
| Cap. volume | 1.39L | 0.56L ➡ a 60 % reduction |

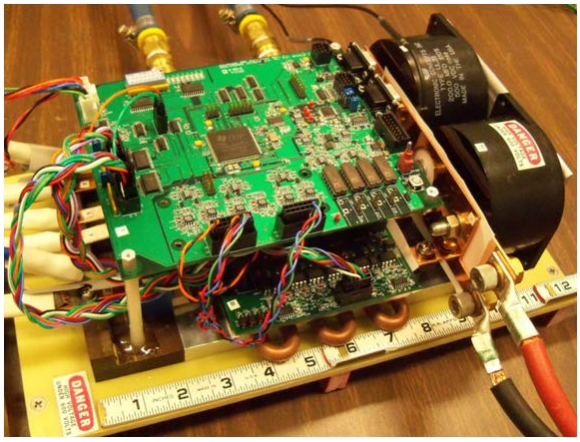

Figure 9. A segmented traction drive inverter.

### B. Test Results with Resistive Load

The prototype was tested first with an inductor-resistor (R-L) load bank with nominal circuit parameters of 0.45 mH and 1.6 Ω. A dc power supply was used to simulate a 300 V battery. For comparison, the prototype was reconfigured as

the baseline VSI and tested at the same load conditions. Fig. 10 shows battery current, $I_{bat}$; load currents, $i_a$, $i_b$, and $i_c$; and capacitor ripple current, $i_{Cbus}$, for the two inverters at a dc input power of 19 kW. The measured capacitor ripple currents are 71.4 Arms for the baseline inverter and 27.4 Arms for the segmented inverter, and the measured peak-to-peak battery ripple currents are, respectively, 45 A and 10 A. These measurements show a reduction of 62% for capacitor ripple current and 78% for battery ripple current with the segmented inverter. Moreover, while the three-phase load current waveforms in the baseline inverter have substantial harmonic components due to the relatively low load inductance, these harmonic components disappeared almost entirely from the current waveforms in the segmented inverter. This is another benefit with the segmented inverter and is important to permanent magnet (PM) motors, which have low inductance. It means a lower switching frequency can be used to increase the inverter efficiency.

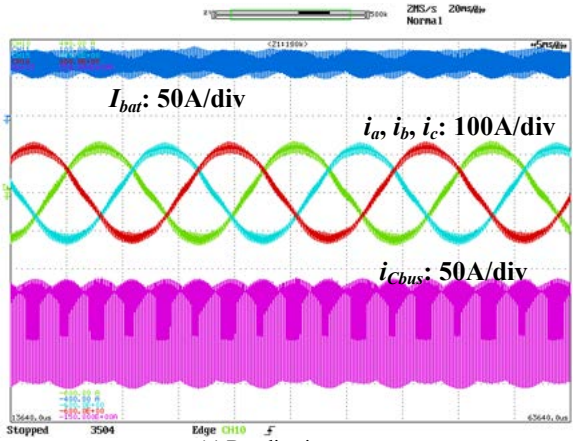


(a) Baseline inverter

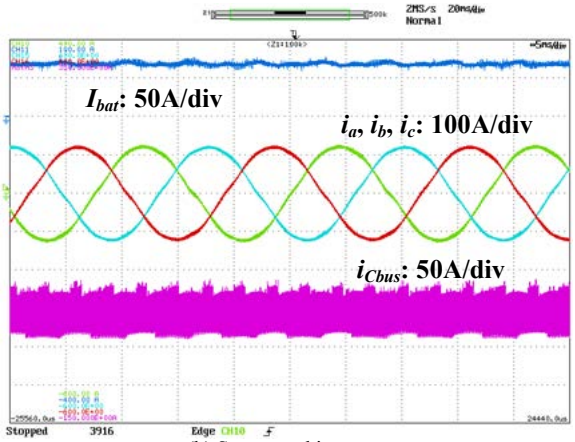


(b) Segmented inverter

Figure 10. Waveforms with an R-L load at dc input power of 19 kW, showing a reduction of 62% for capacitor ripple current and 78% for battery ripple current with the segmented inverter.

Fig. 11 plots the capacitor ripple currents at various levels of input dc power for both the baseline and segmented inverters. The graph shows the segmented inverter offers a significant reduction of capacitor ripple current (in the range of 55% to 75%). Fig. 12 plots the battery ripple currents at various levels of input dc power for both the baseline and segmented inverters. Again, the segmented inverter offers a significant reduction of battery ripple current (in the range of 70% to 80%).

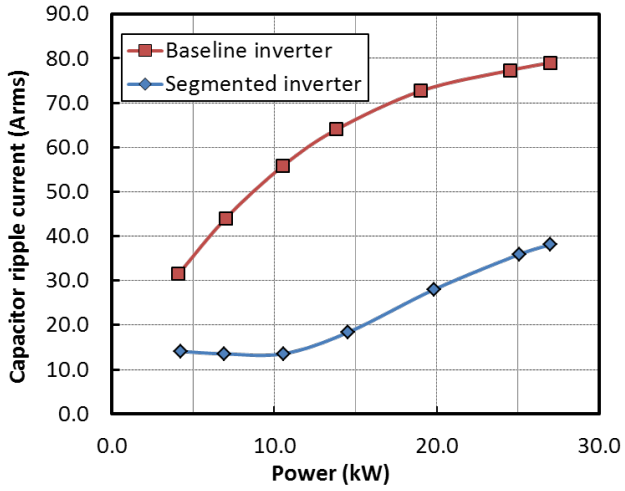


Figure 11. Comparison of capacitor ripple current vs dc input power for an R-L load.

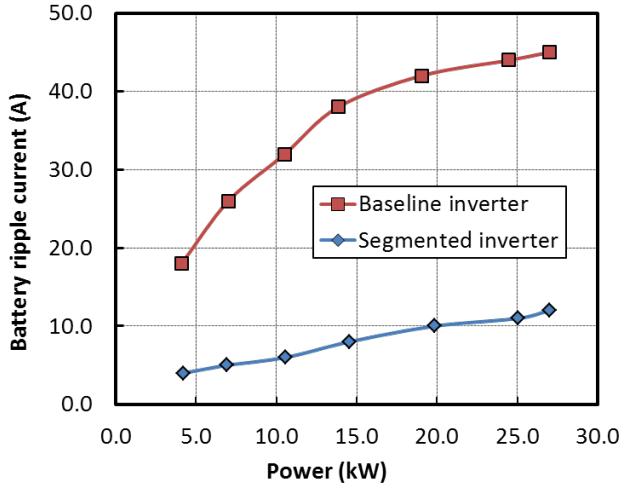


Figure 12. Comparison of battery ripple current vs dc input power for an R-L load.

### C. *Test Results with an Induction Motor*

The prototype was also tested with a commercial, off-the-shelf, induction motor rated at 15 HP, 230 Vrms, 37.5 Arms, 91 Nm, and 1,175 rpm. The motor has six pole pairs and two sets of stator windings in delta connection. Due to the limitation of the maximum dc power supply voltage of 300 V, testes could not be done at the rated speed region. Fig. 13 shows battery current, $I_{bat}$; motor currents, $i_a$, $i_b$, and $i_c$; and capacitor ripple current, $i_{Cbus}$, at 565 rpm and rated torque for the baseline inverter and the segmented inverter. The measured capacitor ripple currents are 31.72 Arms for the baseline inverter and 10.0 Arms for the segmented inverter, and the measured peak-to-peak battery ripple currents are 45 A and 5 A, respectively. These measurements show a reduction of 73% for capacitor ripple current and 89% for

battery ripple current with the segmented inverter. The motor current waveforms also illustrate significantly lower ripple components with the segmented inverter.

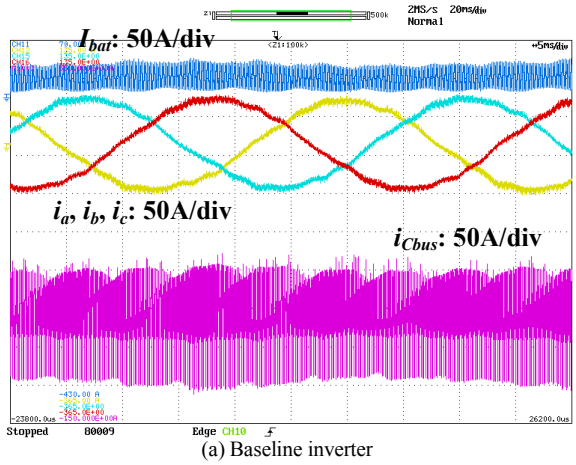


(a) Baseline inverter

(b) Segmented inverter

Figure 13. Waveforms with an induction motor at 565 rpm and rated torque of 91 Nm showing a reduction of 73 % for capacitor ripple current and 89% for peak-to-peak battery ripple current with the segmented inverter.

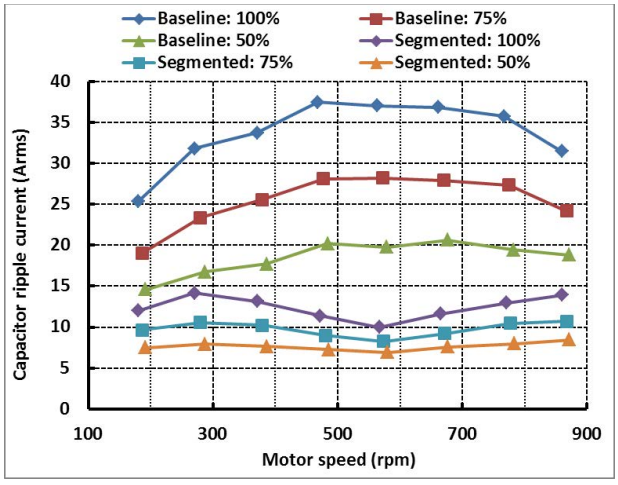


Figure 14. Comparison of capacitor ripple current vs motor speed at loads of 100%, 75%, and 50% of the rated torque of 91 Nm.

Fig.14 plots the capacitor ripple currents at various levels of load torque vs motor speed for both the baseline and segmented inverters. Again, the segmented inverter offers a significant reduction of capacitor ripple current: in the range of 55% to 75% at the rated torque, 50% to 70% at 75% of rated torque, and 50% to 60% at 50% of rated torque.

## IV. CONCLUSIONS

A 60% reduction of dc bus capacitor can be realized with the segmented traction drive system. Test results with both R-L load and an induction motor for a 55 kW segmented inverter prototype compared with those for a 55 kW baseline VSI show a reduction of 55% to 75% in capacitor ripple current, 70% to 90% in battery ripple current, and 60% to 80% in motor ripple current. Moreover, with the segmented inverter a lower switching frequency can be used to increase the inverter efficiency while still maintaining a low level of harmonic components in motor currents, even for low inductance motors such as PM motors.

## REFERENCES


[1] U.S. Department of Energy, Electrical and Electronics Technical Team Roadmap, December 7, 2010, available online at http://www1.eere.energy.gov/vehiclesandfuels/about/partnerships/roadmaps-other_docs.html.

[2] Electronic Concepts, Inc., Electronic Concept Datasheets, available online at http://www.ecicaps.com/capacitors/features/ul3-series-unlytic-lt-sup-gt-reg-lt-sup-gt-ul3-ul31-ul32-ul34-ul35-series.

[3] T. Kawabata and S. Higashino, "Parallel operation of voltage source inverters," *IEEE Trans. Ind. Appl.*, vol. 24, no. 2, pp. 281–287, 1988.

[4] J. Holtz, W. Lotzkat and K-H Werner, "A high-power multitransistor-inverter uninterruptable power supply system," *IEEE Trans. on Power Electronics*, vol. 3, no. 3, pp. 278–285, July 1988.

[5] S. Ogasawara, J. Takagaki, H. Akagi, and A. Nabae, "A novel control scheme of a parallel current-controlled PWM inverter," *IEEE Trans. on Ind. Appl.*, Vol. 28, No. 5, 1992. pp. 1023–1030.

[6] Matsui, K.; Murai, Y.; Watanabe, M.; Kaneko, M.; Ueda, F., "A pulsewidth-modulated inverter with parallel connected transistors using current-sharing reactors," *IEEE Trans. on Power Electronics*, vol.8, no.2, pp.186–191, Apr. 1993.

[7] Z. Ye, D. Borojevic, and F. C. Lee, "Paralleling non-isolated multiphase PWM converters," in Conf. Rec. IAS Annu. Meeting, 2000, pp. 2433–2438.

[8] L. Asiminoaei, E. Aeloiza, J. H. Kim, P. Enjeti, F. Blaabjerg, L. T. Moran, and S. K. Sul, "Parallel interleaved inverters for reactive power and harmonic compensation," 37th IEEE Power Electronics Specialists Conference (PESC '06), pp. 969–976, 18–22 June 2006.

[9] S. K. T. Miller, T. Beechner, and J. Sun, "A comprehensive study of harmonic cancellation effects in interleaved three-phase VSCs," Proc. PESC '2007, pp. 29–35.

[10] D. O. Neacsu, E. Wagner, and B. S. Borowy, "A Simulation Benchmark for Selection of the PWM Algorithms for Three-Phase Interleaved Converters," *IEEE Trans. on Industrial Electronics*, vol. 55, no. 4, pp.1628–1636, April 2008.

[11] D. Zhang, F. Wang, R. Burgos, R. Lai, D. Boroyevich, "Interleaving Impact on AC Passive Components of Paralleled Three-Phase Voltage-Source Converters," IEEE Ind. Appl. Society Annual Meeting (IAS '08), 5–9 Oct. 2008.

[12] J.W. Kolar, T.M. Wolbank, and M. Schrodl, "Analytical calculation of the RMS current stress on the DC link capacitor of voltage DC link PWM converter systems," 9th International. Conf. on Electrical Machines and Drives, Sept. 1999, pp. 81-89.